Tribol Lett (2009) 36:223–231
DOI 10.1007/s11249-009-9476-9

ORIGINAL PAPER

Mechanics of the Ski–Snow Contact

T. Theile · D. Szabo · A. Luthi · H. Rhyner · M. Schneebeli

Received: 17 April 2009 / Accepted: 18 June 2009 / Published online: 1 July 2009

Abstract Two outstanding questions of the ski–snow friction are considered: the deformation mode of the snow and the real contact area. The deformation of hard, well sintered snow in a short time impact has been measured with a special linear friction tester. Four types of deformations have been identified: brittle fracture of bonds, plastic deformation of ice at the contact spots, elastic and delayed elastic deformation of the snow matrix. The latter is the dominant deformation in the ski–snow contact. Based on the measured loading curves the mechanical energy dissipation of snow deformation in skiing on hard snow has been determined and found negligible compared to the thermal energy dissipation. A mechanical model consisting of ice spheres supported by rheological elements (a non-linear spring in series with a Kelvin element) is proposed to model the deformation of snow in the ski–snow contact. The model can describe the delayed elastic behaviour of snow. Coupled with the complete topographical description of the snow surface obtained from X-ray micro computer tomography measurements, the model predicts the number and area of contact spots between ski and snow. An average contact spot size of 110 μm, and a relative real contact area of 0.4% has been found.

Keywords Contact mechanics · X-ray tomography · Surface roughness measurement methods · Snow friction · Snow mechanics

T. Theile · D. Szabo · A. Luthi · H. Rhyner · M. Schneebeli (✉)
WSL Institute for Avalanche and Snow Research SLF, CH-7260 Davos Dorf, Switzerland
e-mail: schneebeli@slf.ch

1 Introduction

It is well known that the slipperiness of ice and snow is due to the formation of a thin meltwater film [1–5]. The frictional heat generated by the rubbing of ice asperities against a slider's base melts the ice and the resulting meltwater lubricates the interface. In very cold conditions when the heat is not sufficient to melt the ice, snow is similar to sand with a high dynamic frictional coefficient of 0.3 [6]. In most natural conditions, however, meltwater lubrication occurs and snow and ice exhibit frictional coefficients as low as 0.01 making skiing, sledging and skating possible.

Snow is a sintered material consisting of mono-crystalline ice grains, which are bonded together [7]. The ice crystals form in the atmosphere. After they fall to the ground they immediately start to sinter together and quickly form a 3D foam-like structure that we call snow. At this stage a process called snow metamorphism starts. During snow metamorphism the size and shape of the ice crystals change. In addition the bonds between the individual crystals grow stronger by sintering. This converts the initially fragile snow into a denser and stronger solid porous material. Depending on how far the metamorphism proceeded, snow densities range from 50 kg/m^3 for freshly fallen snow to 800 kg/m^3 for firn. The latter is close to the density of ice (920 kg/m^3). In Figs. 2 and 3, the 3D microstructure of a high-density snow and its surface is visualized. The surface consists of the same type of grains as the rest of the snow. Only under certain conditions special surface layers, like surface hoar or ice crust occur. In this study, we do not consider such surfaces.

Skiing involves complex and interesting scientific phenomena that attracted the attention of many researchers over the past 100 years [3, 8, 9]. Since the pioneering work

of Bowden, who proposed the idea of meltwater lubrication [1] and introduced polytetrahydrofourene (PTFE) as a superior ski base material [10], the theory of ski friction has been developed to a high degree on a phenomenological basis. The effects of temperature [11], load [11], speed [12], snow type [13], and ski base material [10, 14] on the frictional coefficient of a ski were studied experimentally. In addition qualitative relations were established on an empirical basis. More recently, a fundamental approach to understand the basic physical processes involved in ski friction was started by Glenne [3] and Colbeck [8]. The latter reviewed the individual mechanisms that contribute to the resistance of a ski sliding on snow [8]. These include the plowing of snow in front of the ski, snow compaction below the ski, deformation and fracture of asperities rubbing against the ski, shearing of the meltwater film, drag by dirt particles, and possibly capillary attachments between snow grains and ski base. Currently, these processes, but especially their interactions are poorly understood and a comprehensive description of the ski–snow friction is missing. An attempt to numerically model the friction of a flat polyethylene slider on ice including all physical processes was recently made by Baeurle et al. [15]. They concluded that the most critical parameter in the formation of the meltwater film and thus the frictional coefficient is the real area of contact.

We address two outstanding questions of the ski–snow friction: the deformation mode (elastic, plastic or brittle) of the snow during the contact, and the real contact area between snow and ski base. This is studied by displacement-controlled loading experiments of hard packed snow samples. A ski base is pressed vertically on the snow samples. The analysis of the resulting force–displacement curves gives insight into the dimensions of the occurring forces, displacements and consequently the mechanical energy dissipation during skiing. Before and after the loading experiment a high resolution 3D image of the snow microstructure is captured by X-ray computer tomography [16]. By comparing these images we can visualize the snow deformation. This visualization and the analysis of the force–displacement curves allow a precise identification and quantification of different deformation modes. Furthermore we use the 3D images to characterise the snow surface. The radius and the distribution of the snow grains at the surface are important parameters in the ski–snow contact. In a last step a model of the ski–snow contact is set up. The mechanical response of each grain is modelled by rheological elements. Combining this with the distribution of the grains at the surface, we can model the measured force–displacement curves. The parameters of the rheological element are determined using the Hertzian theory of elastic contacts [17] and a finite element simulation of the mechanical response of the snow structure. The modelled stresses at the contacts exceed the strength of ice by far, so that following simple approximation for the real contact area can be justified: the real contact area is the ratio between normal force and strength of ice [18]. With this approximation, the model predicts besides the number also the size of the contact patches. These are the most important input parameters of a frictional heat simulation.

While our experiment is a vertical impact, in reality the snow grains rub against the ski and experience a shear force in addition to a normal force. Due to the low frictional coefficient, the normal force is much bigger than the shear force and therefore we can neglect the shear deformation in respect of the real contact area and the deformation mode. However, this approximation is valid only in the beginning of the contact. When the accumulated frictional heat melts the top of the ice grains, the contacts get lubricated and the real contact area increases. The amount of meltwater also increases, but it is constantly squeezed out from the contacts. In this region the real contact area is primarily determined by the melting–squeezing mechanism not by the deformation of the grains [15]. The polishing effect of the meltwater lubrication is very pronounced. The relative contact area after the passage of a ski was determined from micrographs of the snow surface. It was found to be around 2–4% [8, 15, 19]. This is one order of magnitude higher than the contact area of 0.4% we determined in our experiments without frictional melting.

2 Experiments

2.1 Snow Sample Preparation

The goal was to prepare reproducible snow samples with structural and mechanical properties similar to that of the snow on racing ski tracks. This corresponds to high density, well packed and well sintered snow with relatively small grains. We used finely grained fresh snow stored for several months in a freezer at –40 °C. Grains with diameters between 250 and 500 μm were sieved into the sample holder in a cold room at $T_{\text{air}} = -6$ °C. The sample holder consisted of a 35 mm diameter solid cylindrical base and a hollow cylinder that fits snugly, but can slide easily up and down on the base. This is illustrated in Fig. 1. The snow was compacted to a density of 500 kg/m^3 in the sample holder. A flat ultra high molecular weight polyethylene (UHMWPE) sheet was used as an impactor. UHMWPE is the base material of modern skis. During compaction the hollow cylinder slides down on the base. Holes drilled into the cylinder prevent pressure build-up in the pore space of the snow. After compaction the snow was allowed to sublimate for approximately 1 h to smoothen the snow surface. It was then covered to prevent further sublimation

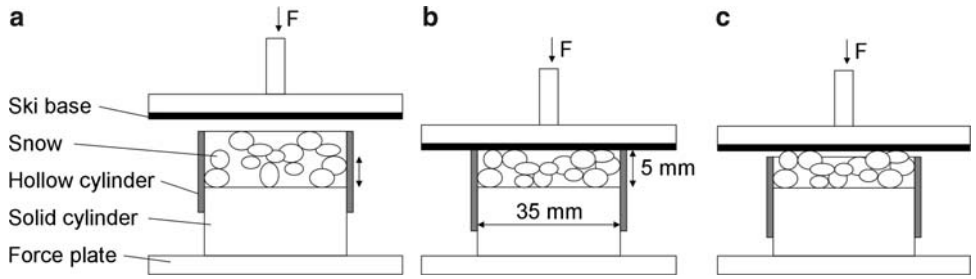

Fig. 1 Sketch of the experimental setup used for sample preparation (**a**, **b**) and the loading experiments (**c**). For sample preparation low-density snow (**a**) is compacted to high-density snow (**b**) by pressing the ski base on the snow. During compaction the hollow cylinder is pushed down by the ski base. It is guided by the solid cylinder. In the experiments the snow is impacted with the ski base. The hollow cylinder is pushed down a bit before running the experiment (**c**) to avoid contact with the ski base

and placed into a chamber where it was stored at –3 °C for 24 h to obtain a high strength, well sintered sample. In total, 16 samples were prepared.

2.2 Tomography Measurements of the Snow Surface

It is possible to obtain a high resolution 3D image of the snow structure with X-ray tomography [16]. A μCT 80 X-ray micro computer tomograph (μCT) from Scanco Medical (Bassersdorf, Switzerland), placed in a cold chamber, was used to characterise the snow surface and to visualise the deformation of snow grains. A special adapter allowed placing the sample holder into the μCT. Images with 18 μm nominal resolution were taken of the top 3 mm of the snow samples. The duration of a scan is approximately 1 h. For image processing and stereological characterisation the raw sinograms of the μCT were transformed into 16-bit images. To reduce the noise, the stacked images were median filtered using a $3 \times 3 \times 3$ kernel and Gaussian filtered using a $5 \times 5 \times 5$ kernel with $\sigma = 1.2$. Finally these images were segmented by thresholding, resulting in a binary image of the snow microstructure. Images were taken before and after the impact experiment. To determine the location and magnitude of the snow deformation, the displacement field between the two images was calculated using particle image velocimetry [20]. Therefore the displacement vector of each voxel is determined by cross-correlating a neighbourhood of the voxel in both images. In addition to this analysis, the 3D images were transformed to 2D surface profiles in order to calculate different roughness properties including average roughness, height distribution, surface density of grains and bearing area ratio. Out of the 16 snow samples, 10 were scanned and analysed with the μCT.

2.3 Impact Loading Experiments

The experimental set-up for the experiments was basically the same as for the sample preparation (Fig. 1c). The snow samples were loaded with a short time vertical impact. The complete loading–unloading cycle takes about 100 ms which roughly corresponds to the passage of a 2-m long racing ski sliding with 20 m/s. The experiments were performed by a linear friction tester (LFT) placed in a cold chamber where temperature was kept at −6 °C. The LFT consists of two high power and high precision computer controlled linear drives that can be programmed to realize any 2D movements. In these specific experiments the horizontal drive is fixed while the vertical drive is programmed to apply an impact on the snow sample placed under the drive. A 2 mm thick flat UHMWPE sheet is glued to the face of the vertical drive and acts as an impactor. The sheet overlaps the snow sample in order to impact the whole sample.

The force and displacement are recorded during the experiment with a high sampling rate. The force is measured with 0.1 N resolution by a Kistler Model 9254 piezoelectric force plate (Kistler, Switzerland) placed under the snow sample. It measures all three force components simultaneously. The displacement is measured with 1 μm resolution by a linear encoder (Renishaw, UK).

The samples were repeatedly impacted several times. By repeating the impact we were able to observe whether the mechanical behaviour of the sample changed and we were able to observe the recovery of the samples. We varied the impact load from 10 N which corresponds to 12 kPa (the maximum pressure under a stationary ski) to 140 N. For the maximal load of 140 N the deformation of the samples was around 20 μm. The sample height was 5 mm. Relating the deformation to the sample height we obtain a strain of 0.004 and a strain rate of 0.04 1/s.

3 Results and Discussion

UHMWPE has a higher mechanical strength than ice, but a lower Young's modulus [21].[1] As a result the ski base deforms elastically during the ski–snow interaction while

[1] For material properties of UHMWPE refer to www.uhmwpe.org

the ice fails when the stress exceeds its compressive strength. This makes the skis wear resistant and long lasting.

Let us consider the impact of a flat UHMWPE sheet (slider) on hard snow. What would we expect as a result of such an impact: first, the top ice grains come into contact with the slider. As long as the load on the grains is not too excessive the contacts are elastic. The area of the contact patch can be calculated from the Hertzian contact theory. Since the grains are part of a flexible snow matrix, they are not fixed in space. They are pushed down by the contact force. As the contact force increases the grains start to fail. Either the contact pressure reaches the compressive strength of ice, or their bonding in the matrix is not strong enough. In the former case the ice yields until the contact stress drops below the compressive strength. In the latter case the bonds that support the grains yield, and the grain is displaced from the surface as a whole. The failure of grains continues until the number of grains in contact and the real contact area is high enough to support the load. We tried to visualise the deformation of the grains in the snow with the μCT.

The 3D images of the surface of a snow sample before and after an impact experiment are shown in Fig. 2. The absolute displacements of most surface points are around zero. Except for a very few surface grains no deformation is visible. This confirms our expectation that on hard snow the ski–snow interaction is limited to the very top of the snow. All of the grains that show a visible permanent deformation originally rise well above the average surface level. These grains come into contact with and loaded by the slider first. They experience excessive loads. Their bonds fail and they fall down. One example of such a grain is shown in Fig. 3. In its final position the top of this grain is under the surface. This shows that its bonds failed completely by brittle failure and the grain fell down instead of having been pushed down by the slider. The sharp transition from the big displacement of the grain to no displacement of the neighbouring grains confirms this. Beside the brittle failure of the bonds the grain itself might deform plastically and forms new bonds in its new position. The grain does not carry any load after failure. The cracking of the bonds of these grains was also observed in the loading experiments: In Fig. 4 the oscillations in the

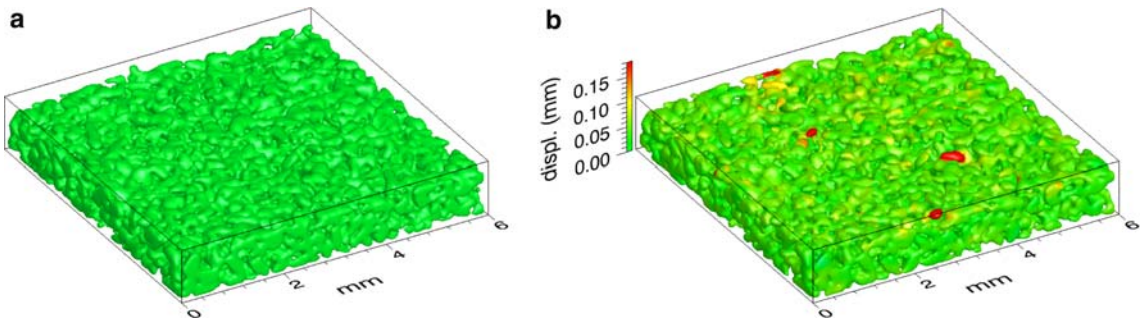

Fig. 2 3D image of a 6 × 6 mm section of the snow surface before (**a**) and after (**b**) the loading experiment. The absolute displacements between the two images, calculated by particle image velocimetry, are colour-coded in (**b**). No considerable deformation can be seen as a result of the 150 kPa impact. Only isolated grains (in red) that originally rise above the average surface level deform considerably

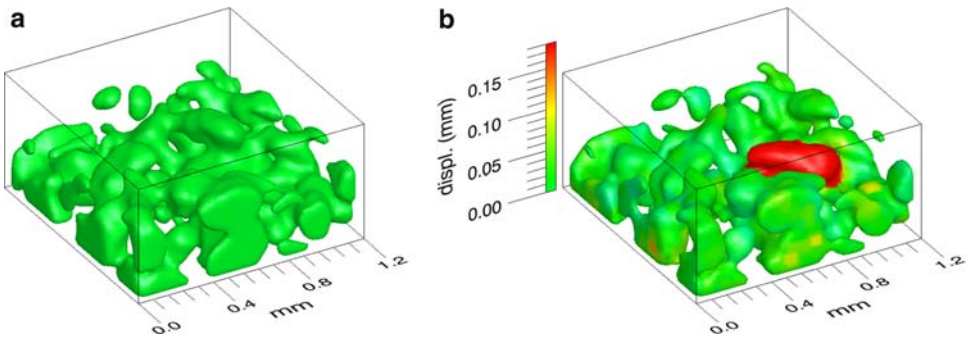

Fig. 3 Close-up of the deformation of a grain that originally rises well above the surface (image **a**). It fails under the impact and falls down (image **b**). In its new position it is below the average surface level indicating brittle failure. Another evidence of brittle failure is that the immediate neighbourhood of the grain shows zero deformation. For a plastic deformation we would expect a smooth transition similar to the deformation pattern shown in Fig. 7

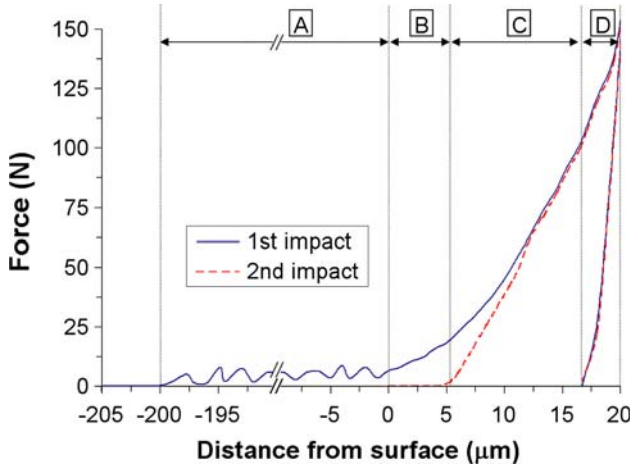

Fig. 4 Schematic force–displacement curves of two subsequent impact experiments with the same maximum force. Four different deformation modes (A–D) can be identified. The first impact shows an oscillation of the force from −200 μm to 0 μm (A). This is the brittle failure of surface grains. The surface is defined as the point from which the force signal starts to rise continuously. After the maximum force is reached an elastic recovery of 3 μm occurs during the unloading of the sample (D). The point where the second impact touches the new surface gives information about the delayed elastic recovery of the snow matrix (C) and the total permanent deformation (A + B) of the snow. Thereof about 5 μm are caused by the flattening of the grains which are in contact with the ski (B)

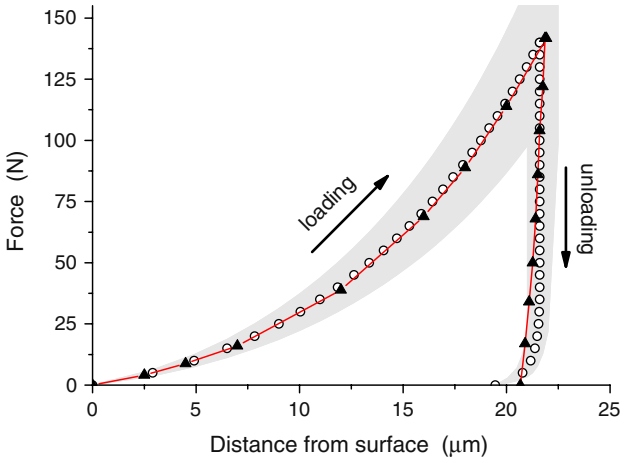

Fig. 5 Average measured force–displacement plot of the impact loading of 10 hard snow samples (*open circles*). The grey band shows the variation of the measured loading curves (approximately 20%). The whole loading–unloading cycle takes approximately 100 ms. Subsequent loadings of a sample follow exactly the same curve. The calculated plot based on our model shown in Fig. 6 is also shown (*solid triangles and line*)

force in the initial phase of the loading are caused by the brittle failure of the bonds. This occurred only in the first loading of the sample, subsequent loadings showed a smooth increase of the force. The failure of these weakly bonded surface grains is a permanent deformation.

Another expected permanent component of the deformation is the failure of ice on the top of the grains. This deformation is too small to be visible on the μCT images, but it appears in the loading experiments as a shift between the first and subsequent loadings. In Fig. 4 it is labelled as phase B. It is approximately 5–10 μm. Due to the low number of grains actually in contact with the ski base very high local stresses develop on the top of the grains. The stress far exceeds the compressive strength of ice (around 10 MPa at high deformation rates [21, 22]). As a result a localized failure of the ice is inevitable. The failure mechanism is probably a mixture of plastic flow, microcracking and possibly pressure melting depending on the actual stress and strain rate experienced by the grain. Failure of the ice continues until the average stress drops below the strength of ice.

The permanent deformations of the snow discussed above only appear in the first loading of a snow sample. After this first impact the surface is 'prepared' to take the load without further permanent deformation. In subsequent loadings the force rises and drops smoothly. This can be observed in the force–displacement curve of the second impact in Fig. 4. This smooth force–displacement curve is plotted in Fig. 5. The curve shown is the average of measurements on 10 different samples. Different samples showed 20% deviation which is quite reasonable in experiments with snow. Two interesting features are immediately noticeable. One is the small deformation. The snow is very hard, the total deformation is only 22 μm at 140 N (corresponds to 150 kPa). Another interesting result is that the loading and unloading follow different paths. The loading curve forms a hysteresis loop. This indicates permanent deformation in the snow. Subsequent loadings of a sample, however, closely follow the same curve. The position of the surface where the force starts to rise remains exactly the same. It seems that the sample recovers the strain after unloading and regains its undeformed state. In Fig. 4 this recovery is labelled as phase C. This behaviour is well known in ice mechanics. It is referred to as primary creep or delayed elasticity [23]. It has never been studied for snow. Only for crushed ice Singh et al. [24] describe this behaviour. It is expected to be more pronounced in snow than in case of polycrystalline ice since it is known to be greatly enhanced with increased porosity [25]. Nevertheless it is very surprising that delayed elasticity is present at such a high strain rate (0.04 1/s) and that the deformation is fully recovered. This is a clear indication how significant delayed elasticity can be in snow. In ice one would expect brittle failure at this strain rate. Polycrystalline ice behaves brittle at strain rates higher than 10^{-3} 1/s [23]. Unlike in ice, however, the grains have a high mobility in the snow matrix. They can freely move by grain boundary sliding, which is the underlying mechanism of delayed elasticity [23, 25]. The high mobility of the grains then leads to an

effective stress relaxation mechanism, and hence improved delayed elasticity.

The reverse creep of delayed elasticity is slower than the withdrawal of the impactor in our experiments. As a result the unloading part of the curve shows the purely elastic part of the deformation. This is only 2–3 μm and includes both the elastic deformations of the ski base and the snow matrix.

Pressure melting and premelting of the ice cannot explain the observed hysteresis in the loading curve. In case of pressure melting a melting–refreezing cycle of the top of the loaded snow grains could result in a hysteresis, but in reality the ice fails well before it could melt. According to the Clausius–Clapeyron equation the melting point of ice changes with pressure as 13.35 MPa/K. All of our experiments were conducted at −6 °C. Lowering the melting point of ice to −6 °C requires around 80 MPa which is eight times higher than the compressive strength of ice (10 MPa) at high strain rates.

It has been shown by different experimental techniques that a naturally occurring quasi liquid layer (QLL) exists on the surface of ice close to the melting point [26]. However, the thickness of the QLL is very small compared to the displacements in our measurements. Even for ice with a high impurity content (which is known to enhance premelting) it does not exceed 100 nm at −6 °C [27]. In addition, the relative humidity in our cold rooms during the experiments was between 30 and 50%. In such a low humidity we do not expect to have a QLL on the surface of the top snow grains [28].

Nano- and micro-indentation experiments on ice show a recovery of the ice surface similar to our observations. In nanoindentation the heeling of the surface is attributed to the flow of the QLL [29]. As we mentioned above, in the dry air of our cold rooms we do not expect a QLL present at −6 °C. In addition, the length scale of these experiments is very different. The small volume of the imprint of the microscope tip is filled up quickly, but it is insufficient to account for the 20–30 μm deformation in our experiments. In micro-indentation of ice the indent is filled very slowly (on the time scale of hours) by newly growing ice grains [30]. In our experiments the snow is recovered after 1 min, a very different time scale. While we cannot exclude that some of the processes discussed above present in our experiments, delayed elasticity seems to be the dominating underlying mechanism of the hysteresis observed in our loading experiments.

The energy dissipated through snow deformation in skiing can be estimated from the loading curve shown in Fig. 5. The total energy dissipation of a ski, P is simply $P = \mu v F_n$ where μ is the frictional coefficient of the ski on snow, v is velocity and F_n is the normal load. For a racing ski, $\mu = 0.1$, $v = 20$ m/s and $F_n = 400$ N which yields 800 J/s. The area of the hysteresis loop (860×10^{-6} J) corresponds to the energy lost to compaction of around 10^3 mm^2 of snow. A 7-cm wide ski, moving with 20 m/s, compacts 1.4×10^6 mm^2/s of snow. Hence the energy lost to snow compaction of this ski amounts to approximately 1 J/s, 0.1% of the total energy dissipation. Therefore, snow deformation can be neglected on a hard ski track leaving thermal energy dissipation the dominant process.

Based on our impact experiments it is possible to construct a mechanical model of the ski–snow contact which will serve as an input to thermal simulations for calculations of meltwater generation. The model includes only the non-permanent part of the deformation, namely the elastic deformation of the ski base and snow, and the delayed elastic deformation of the snow. Figure 6 shows the schematic representation of the model. The mechanical behaviour of the surface grains and their support by the snow matrix are modelled with rheological elements. Each grain is supported with a spring (K_1) and a Kelvin element (K_2, c_v) in series. This is the simplest rheological model which can describe the desired deformation mode. The spring element (K_1) includes the two elastic components of the deformation: the contact between the top of the grains and the ski base, and the elasticity of the snow matrix. The former can be calculated from the Hertzian theory of elastic contacts [17]:

$$F_n(\delta) = \frac{4}{3} E^* \sqrt{R} \delta^{3/2} \tag{1}$$

Here the normal force, F_n is expressed as a function of deformation, δ. E^* is the effective combined modulus and R is the combined radius of UHMWPE and ice, respectively. R includes the radius of the ice spheres that come into contact with the flat UHMWPE ski base ($R_{\mathrm{UHMWPE}} = \infty$). This contact radius was determined from the μCT images. An algorithm was used that fits a sphere to the top section of all surface grains. Therefore not the whole grain, only its top part is used to obtain the radius. A value of 0.18 mm was obtained which is surprisingly close to the average radius of the ice grains used in the sample preparation (0.175 mm). With this, and the Young's moduli of 9100 and 1200 MPa for ice and UHMWPE, respectively, Eq. 1 becomes $F_n(\delta) = 680.52$ N mm$^{-3/2}$ $\delta^{3/2}$. The implementation of this non-linear relation requires a non-linear spring (K_1) in the mechanical model shown in Fig. 6.

In addition to the contact between ski base and ice grains the spring element in the model includes the purely elastic component of the deformation of the snow matrix. This was calculated with finite element simulations. A 1.8×1.8 mm^2 section of the 3D μCT images of the snow samples was converted into a discrete finite element mesh with ANSYS ICEM CFD.[2] The mesh was then used to

[2] For further information on CADFEM products refer to www.ansys.com

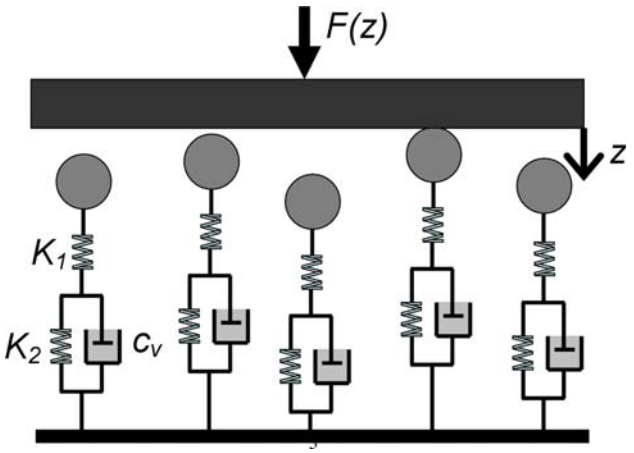

Fig. 6 Schematic presentation of the mechanical model of the ski–snow interface. Only surface grains are considered all having the same (average) radius. The grains are supported by elastic springs and dashpots that represent the snow matrix

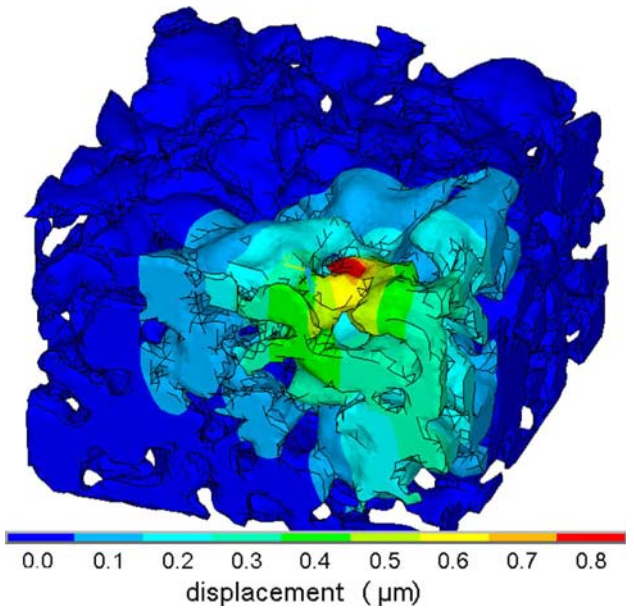

Fig. 7 Contour plot of the vertical displacement of a typical finite element simulation of the stiffness of surface grains in the snow. It was calculated with a linear structural analysis in the finite element program ANSYS. A realistic load of 0.3 N was applied on this grain. With the simulated displacement of 0.8 μm, a stiffness of 0.375 N/μm results for this grain

calculate the stiffness of 50 randomly chosen surface grains of the snow with the commercial finite element software ANSYS (see footnote 2). In these simulations a load is applied on the top of a surface grain and the resulting displacement is calculated by linear structural analysis. The result of a typical simulation is shown in Fig. 7. The average stiffness of the grains was found to be 0.53 N/μm, a surprisingly high value. In order to check the validity of the simulations we calculated the Young's modulus of a

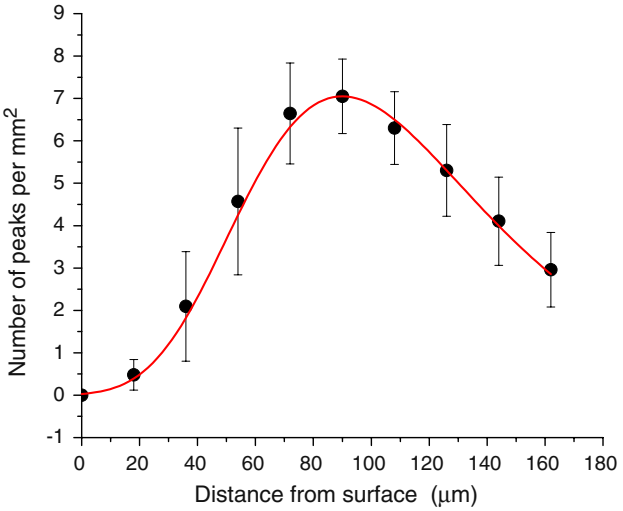

Fig. 8 The number of peaks per unit area in the snow samples as a function of depth. It was calculated from the μCT images. Error bars show standard deviation. The red line represents the best fit of a Weibull distribution

sample with a density of 520 kg/m^3. We obtained 1200 MPa which corresponds well with measured values [31]. In addition we verified that the dependence on system size is negligible.

The Kelvin element (K_2, c_v) in the model is responsible for the delayed elasticity and the majority of the deformation. Since no measurements of delayed elasticity exist for snow in the literature the parameters of the spring and dashpot (i.e. the spring constant, K_2 and damping coefficient, c_v) are unknown. They must be determined by fitting the model to the measured loading curve. This requires the height distribution of the grains on the snow surface. We determined this from the μCT images with an algorithm that finds the coordinates of the peak of each surface grain. The number of grains per unit area as a function of depth, $n(z)$ is plotted in Fig. 8. The curve has a maximum at around 0.09 mm, half the average grain radius. Note the scale of the x axis. The resolution of the μCT is 18 μm, only slightly smaller than the total deformation of the snow. Therefore, the fitted curve must be used to extrapolate values close to the surface. With this the total force $F(Z)$ as a function of depth Z can be calculated from

$$F(Z) = A * \int_0^Z \frac{\mathrm{d}n}{\mathrm{d}z}(z) * f_Z(z)\mathrm{d}z \qquad (2)$$

where A is the area of the sample and $f_Z(z)$ denotes the force exerted by a single grain originally being in a depth of z and finally pushed down to Z. The total force was calculated numerically.

Since the displacement of the impactor follows a non-linear curve over time, the deformation rate the grains

experience, depends on the depth z. Therefore, the function $f_Z(z)$ is different for each Z and it must be calculated individually for each Z. In practice, we calculated $f_Z(z)$ with ANSYS for eight different Z values. To this end a transient analysis was performed on the rheological model in Fig. 6. The real displacement of the UHMWPE impactor over time in the experiments was applied on the model and the reaction force calculated. The total force could then be calculated for the eight Z values.

The parameters of the Kelvin element in the model (K_2 and c_v) are unknown. The fit shown in Fig. 5 was obtained with the following parameters of the Kelvin element: $K_2 = 26.2$ N/mm and $c_v = 550$ kg/s, respectively. The unloading part of the curve could be determined in the same way using the displacement of the impactor during withdrawal. The parameters of the Kelvin element are material constants of the snow. They describe the delayed elasticity of hard snow.

The force on a single grain can be obtained by dividing the total force by the number of grains shown in Figs. 5 and 8, respectively. It is shown in Fig. 9. In the beginning of the loading (i.e. close to the surface) only a few grains are in contact with the ski. The force per grain is enormous. This is when grains and bonds in the snow fail. As more and more grains come into contact with the ski the force per grain decreases and eventually reaches a constant value of 0.3 N. This force is still remarkably high. The Hertzian contact theory predicts an average stress of 50 MPa in the contact patch, if the deformation was purely elastic. As the strength of ice is considerably below 50 MPa, the ice on the top of the grains certainly fails. The failure will increase the area of the contact patch until the average stress drops below a critical value. Assuming that this critical stress is the penetration hardness of ice, which is approximately three times the compressive strength [17],

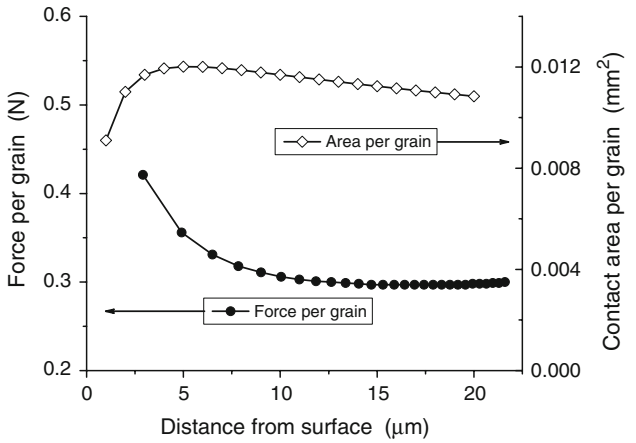

Fig. 9 Force per grain (*solid symbols*) and contact area per grain (*open symbols*) as a function of depth. Both force and area have a relatively constant value

the real contact area can be calculated from the ratio of normal force to penetration hardness. This approach is similar to the calculation of the real contact area between metals [18]. The resulting real contact area of one grain is shown in Fig. 9. A value of 0.011 mm^2 corresponds to a contact patch radius of 55 μm. The relative real contact area between snow and ski is found to be around 0.4%. This is the contact area at the front part of the ski right after the front impacts the snow. It will increase when melting starts.

An estimation of the permanent deformation of the top of the snow grains after the first impact can also be made from the contact area per grain. A lower and upper limit of the deformation can be given from simple geometrical considerations. The top of the grain is flattened by the high load until a contact patch radius of 55 μm is reached. This can be achieved by either pushing the ice aside to form a plateau or by shaving the top of the grain completely off. The former approach gives a lower limit of the deformation, and results in 4 μm. The latter predicts 9 μm, and it is an upper limit. These estimates are very close to the 5–10 μm permanent deformation observed in the experiments (phase B in Fig. 4).

4 Conclusions

The ski–snow contact is a complicated mechanical process. Even without sliding the effect of the impact of a ski on the snow is very complex. Four types of deformation have been identified during a high speed impact on hard snow with a maximum pressure of 150 kPa:

- The brittle failure of the bonds of some surface grains that come into contact with the ski first. These grains are displaced from the surface and do not bear any load after failure.
- Highly localized failure of the ice on the top of the grains at the contact with the ski. This type of failure continues until the contact stress drops below the strength of ice and it is 5–10 μm. It is probably a mixture of plastic flow and micro-cracking.
- Elastic deformation of the ski base and snow matrix. The former is 2–3 μm, the latter is around 0.5 μm, practically negligible.
- Delayed elastic deformation of the snow matrix. This deformation is fully recovered after unloading. It is approximately 20 μm.

The first two types of deformation are permanent, while the two other are fully recoverable.

A mechanical model consisting of basic rheological elements was constructed that describes the recoverable part of the snow deformation. The model can properly

describe the deformation of the snow as a result of an impact. Coupled with the topography of the snow surface obtained from μCT measurements, the number and area of the contact spots can be determined. A remarkably constant value of 0.3 N as the force on one grain during the loading, and 0.4% relative real contact area between ski and snow were found. These values serve as important input parameters in the thermal simulation of meltwater lubrication.

Acknowledgements This study is part of a joint research effort conducted together with the Christian Doppler Laboratory "Biomechanics in Skiing" headed by Erich Müller, University of Salzburg. The project was financially supported by Stöckli Swiss Sports and Atomic Austria GmbH. We thank the two anonymous reviewers for their constructive and detailed comments.

References

1. Bowden, F.P., Hughes, T.P.: The mechanism of sliding on ice and snow. Proc. R. Soc. Lond. Math. Phys. Sci. **172A**, 280–298 (1939)
2. Ambach, W., Mayr, B.: Ski gliding and water film. Cold Reg. Sci. Technol. **5**, 59–65 (1981)
3. Glenne, B.: Sliding friction and boundary lubrication of snow. J. Tribol. **109**, 614–617 (1987)
4. Tusima, K., Yosida, Z.: The melting of ice by friction. Low Temp. Sci. **A27**, 17–30 (1969)
5. Colbeck, S.C., Najarian, L., Smith, H.B.: Sliding temperatures of ice skates. Am. J. Phys. **65**, 488–492 (1997)
6. Bowden, F.P.: Friction of snow and ice. Proc. R. Soc. Lond. Math. Phys. Sci. **217A**, 462–478 (1953)
7. Colbeck, S.C.: Sintering in a dry snow cover. J. Appl. Phys. **84**, 4585–4589 (1998)
8. Colbeck, S.C.: A review of the friction of snow skis. J. Sport Sci. **12**, 285–295 (1994)
9. Lind, D., Sanders, S.P.: The Physics of Skiing. Springer-Verlag, New York (1996)
10. Bowden, F.P.: Friction on snow and ice and the development of some fast-running skis. Nature **176**, 946–947 (1955)
11. Buhl, D., Fauve, M., Rhyner, H.: The kinetic friction of polyethylene on snow: the influence of the snow temperature and the load. Cold Reg. Sci. Technol. **33**, 133–140 (2001)
12. Colbeck, S.C.: Kinetic friction of snow. J. Glaciol. **34**, 78–86 (1988)
13. Hamalainen, T., Spring, E.: Influence of snow hardness on ski friction. Comment. Phys.-Math. **76**, 1–17 (1986)
14. Colbeck, S.C., Perovich, D.K.: Temperature effects of black versus white polyethylene bases for snow skis. Cold Reg. Sci. Technol. **39**, 33–38 (2004)
15. Baurle, L., Kampfer, T., Szabo, D., Spencer, N.D.: Sliding friction of polyethylene on snow and ice: contact area and modeling. Cold Reg. Sci. Technol. **47**, 276–289 (2007)
16. Schneebeli, M., Sokratov, S.A.: Tomography of temperature gradient metamorphism of snow and associated changes in heat conductivity. Hydrol. Process. **18**, 3655–3665 (2004)
17. Johnson, K.L.: Contact Mechanics. Cambridge University Press, Cambridge (1985)
18. Bowden, F.P., Tabor, D.: The Friction and Lubrication of Solids. Clarendon Press, Oxford (1950)
19. Huzioka, T.: Studies on the resistance of a snow sledge, 5. Friction between snow and a plastic plate. Low Temp. Sci. **A20**, 159–180 (1962)
20. Pudasaini, S.P., Hutter, K.: Avalanche Dynamics: Dynamics of Rapid Flows of Dense Granular Avalanches. Springer-Verlag, New York (2007)
21. Kim, H., Keune, J.N.: Compressive strength of ice at impact strain rates. J. Mater. Sci. **42**, 2802–2806 (2007)
22. Petrovic, J.: Mechanical properties of ice and snow. J. Mater. Sci. **38**, 1–6 (2003)
23. Sanderson, T.J.O.: Ice Mechanics: Risks to Offshore Structure. Graham and Trotman Ltd., London (1988)
24. Singh, S.K., Jordaan, I.J.: Constitutive behaviour of crushed ice. Int. J. Fract. **97**, 171–187 (1999)
25. Sinha, J.K.: Grain boundary sliding in polycrystalline materials. Philos. Mag. **40A**, 825–842 (1979)
26. Wettlaufer, J.S.: Ice surfaces: macroscopic effects of microscopic structure. Phil. Trans. R. Soc. Lond. A **357**, 3403–3425 (1999)
27. Wettlaufer, J.S.: Impurity effects in the premelting of ice. Phys. Rev. Lett. **82**, 2516–2519 (1999)
28. Petrenko, V.F.: Surface of ice. U.S. Army Cold Regions Research and Engineering Laboratory, CRREL, Report 94-22 (1994)
29. Pittenger, B., Fain S.C., Cochran, M.J., Donev, J.M.K., Robertson, B.E., Szuchmacher, A., Overney, R.M.: Premelting at ice-solid interfaces studied via velocity-dependent indentation with force microscope tips. Phys. Rev. B **63**, ARTN 134102 (2001)
30. Golovin, Y.I., Shibkov, A.A., Shishkina, O.V.: Effect of complete restoration of the ice surface after indentation in the temperature range 243–268 K. Phys. Solid State **42**, 1287–1289 (2000)
31. Shapiro, L.H., Johnson, J.B., Sturm, M., Blaisdell, G.L.: Snow mechanics: review of the state of knowledge and applications. U.S. Army Cold Regions Research and Engineering Laboratory, CRREL, Report 97-3 (1997)